

Magnetic Barrier Effect on Operating Performances of Switched Reluctance Motor

J.Y. Lee¹, K.Y. Nam¹, Jung-Pyo Hong¹, J. Hur²

¹ Department of Electrical Engineering, Changwon National University

#9 Sarimdong, Changwon, Gyeongnam, 641-773, Korea, Tel: (+8255)2625966, Fax: (+8255) 2639956

² Precision Machinery Research Center of Korea Electronic Technology Institute, Korea

E-mail: jyecad@korea.com, giyongnam@empal.com, jphong@changwon.ac.kr, jinhur@keti.re.kr

I. INTRODUCTION

In reluctance motors, the design of magnetic barriers or salient poles is an important portion through overall design process because the number or the configuration of them affects d- and q-axes inductances, which can change torque characteristics such as average torque and torque ripple. Most papers about reluctance motor design, however, deal either magnetic barrier or salient pole only.

Therefore, this paper deals with two kinds of novel shape doubly salient switched reluctance motors (SRMs), which have magnetic barriers, to exam the effect of magnetic barrier on operating performances of SRMs. The motor named SBSRM has magnetic barriers whose shapes are similar to those of transverse-laminated synchronous reluctance motor, and the other named PBSRM has partial magnetic barriers of SBSRM.

The configurations and common specifications of the two barrier-type SRMs and a prototype, which has no magnetic barriers, are introduced at first. Then, the time-stepping method, which has been used for dynamic simulation, is explained for magnetic characteristic analysis of the three motors. Finally, the inductance profiles of each motor are presented, and operating performances are compared and contrasted.

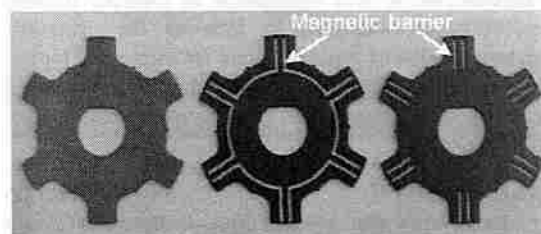
II. SPECIFICATIONS AND CONFIGURATIONS

A prototype, which is made for study at Changwon National University in Korea, has been used as the basis for designing the barrier type motors used in this comparison. Table I shows the common specifications. The two barrier-type SRMs are identical with the prototype except the existence of magnetic barrier in the rotor. The switch on/off phase voltage and angle are the condition at the rated operating point, and the base angle 0° is the position that stator and rotor poles are unaligned.

The rotors of the prototype and barrier-type motors are shown in Fig. 1. The magnetic barriers of SBSRM are optimised by response surface methodology to improve torque characteristics [1]. The shape is modeled on transverse-laminated synchronous reluctance motor. If the barrier is only in the rotor pole, it is PBSRM. This shape is designed by considering magnetic flux paths of general SRMs because main flux path directly crosses the rotor when the same phase winding is on the opposite side and switches are turned on and off by phases.

TABLE I COMMON SPECIFICATIONS

Parameter	Constraint
Number of poles	Stator : 8, Rotor : 6
Stator outer diameter	90.0 mm
Rotor outer diameter	46.8 mm
Rotor stack length	95.0 mm
Air gap length	0.4 mm
Stator pole arc	18.5°
Rotor pole arc	19.0°
Switch turn on/off phase voltage and angle	150/-150 V 5/ 20°
Rated speed	1800 rpm



(a) Prototype (b) PBSRM (c) SBSRM

Figure 1. Fabricated rotor configurations

III. FIELD COMPUTATION METHOD

The electromagnetic characteristics of the SRMs are computed by time-stepping method. For the time-stepping method, 2D finite element method is used to model the nonlinear magnetic field of the SRMs, and coupled to the power electronic circuit. The method can also be called coupled field-circuit method, and the accuracy is proved by comparison of the simulation and the experiment results in [1] and [2]. Since the comparison result in [1] is for the prototype in Figure 1, verification of the method will be omitted in this paper.

IV. COMPARISONS OF PERFORMANCES

The winding inductance $L(\theta, i)$ depends on rotor position θ and winding current i . Fig. 2, therefore, shows inductance profiles of the motors for θ and i . Each inductance profile is at a constant current. The magnitude of the inductances is similar, but the shapes of profiles are quite different from each other. The barriers make inductance profiles varied from the curved line shape to distorted or straight one. This variation can improve the

characteristics of current and torque ripple as shown in Fig. 3, and this result is obtained under the drive condition as shown in Fig. 4. The digits show the ranges during switch-on, and the prototype is set 100% as a base value. The ripple will be similar to these results although current and torque ripple, defined as range over average value, can be changed by speed, switch turn-on angle, the difference between switch turn-on and off angle, etc.

Table II shows the several comparisons of performances at rated operating point. All of the average torque, torque ripple, and the average torque per current as efficiency are improved in SBSRM. Magnetic radial force, which causes mechanical vibration [3], is decreased by 10%, and the average torque per current is increased by 5% in PBSRM.

V. CONCLUSIONS

In this paper two barrier-type SRMs are investigated to improve the operating performances of the prototype. The barriers influence electromagnetic characteristics of the motors, and the results are presented. The results show the fact that barriers can also be an effective design variable for SRMs. In addition, it is expected that the two barrier-type motors can be used as standard or example models when SRMs are designed to improve the operating performance. SBSRM types are good for improving torque ripple, and PBSRM types for efficiency. More detailed comparison and explanation will be presented in the extended paper.

VI. REFERENCES

- [1] Young-Kyoun Kim, Ji-young Lee, Jung-Pyo Hong, and Jin Hur, "Optimization of Barrier type SRMs with Response Surface Methodology Combined with Moving Least Square Method," *International Symposium on Electromagnetic Fields in Electrical Engineering (ISEF2003)*, vol.2/2, pp659-664, September 18-20, 2003, Maribor, Slovenia.
- [2] Longya Xu and Eric Ruckstader, "Direct Modeling of Switched Reluctance Machine by Coupled Field-Circuit Method," *IEEE Trans. on Energy Conversion*, vol. 10, No. 3, pp446-454, September, 1995
- [3] Jung-Pyo Hong, Kyung-Ho Ha, and Ju Lee, "Stator Pole and Yoke Design for Vibration Reduction of Switched Reluctance Motor," *IEEE Trans. on Magnetics*, vol. 38, No. 2, pp929-932, March, 2002

TABLE II COMPARISON OF CHARACTERISTICS (UNIT: %)

	Prototype	PBSRM	SBSRM
average torque	100	99.78	102.72
torque ripple	100	85.68	79.64
magnetic radial force at switch turn-off	100	90.49	94.51
current (rms)	100	94.51	101.58
maximum current	100	88.78	94.90
average torque per current	100	105.57	101.11

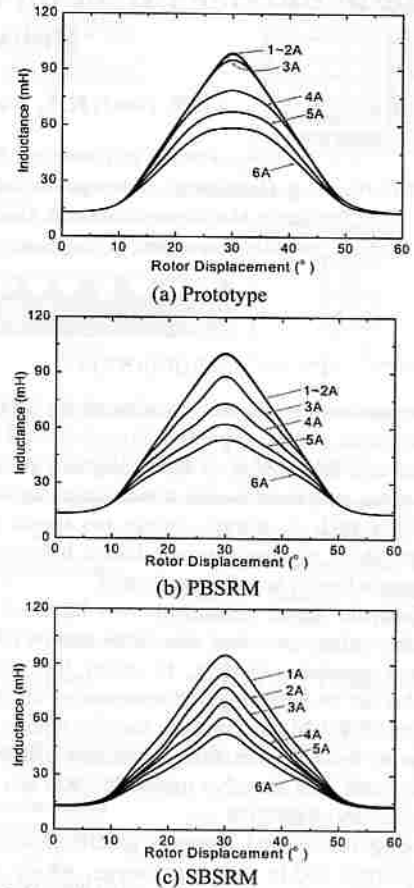


Fig. 2 Variation of inductances for rotor displacement and current

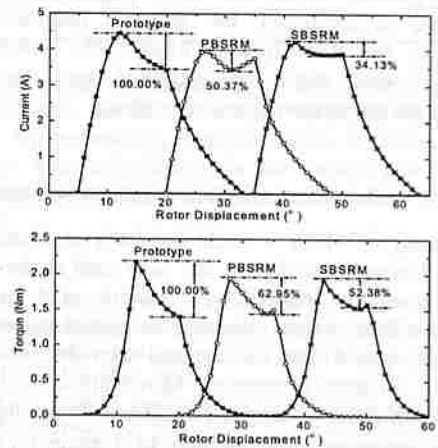


Fig. 3 Currents and torques at rated operating point

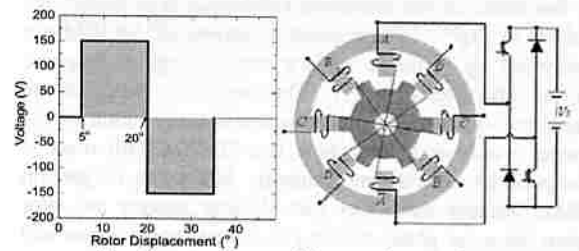


Fig. 4 Input voltage and inverter for one phase

Magnetic Barrier Effect on Operating Performances of Switched Reluctance Motor

¹Ji-Young Lee, ¹Ki-Yong Nam, ¹Jung-Pyo Hong, Senior Member, *IEEE*, ²Jin Hur

¹Department of Electrical Engineering, Changwon National University
#9 Sarimdong, Changwon, Gyeongnam, 641-773, Korea, phone: (+8255)2625966, fax: (+8255) 2639956

²Precision Machinery Research Center of Korea Electronic Technology Institute, Korea
e-mail: jyecad@korea.com, givongnam@empal.com, jphong@changwon.ac.kr, jinhur@keti.re.kr

Abstract — This paper deals with two kinds of novel shape switched reluctance motors (SRM) with magnetic barriers in order to improve operating performance of prototype. The so-called coupled field-circuit method is used to analyze the complicated flux pattern of the SRM and its terminal characteristics simultaneously. After experimental results are presented to prove the accuracy of the analysis method, the several analysis results of each model are compared and the improved rotor shape is presented.

I. INTRODUCTION

In reluctance motors, the design of magnetic barriers or salient poles is an important portion through overall design process because the number or the configuration of them affects d- and q-axes inductances, which can change torque characteristics such as average torque and torque ripple. Most papers about reluctance motor design, however, consider only one of the magnetic barriers and salient poles to improve the characteristics.

Therefore, this paper deals with two kinds of novel shape doubly salient switched reluctance motors (SRM), which have magnetic barriers, to exam the effect of magnetic barrier on operating performances of SRM. The motor named BSRM has magnetic barriers whose shapes are similar to those of transverse-laminated synchronous reluctance motor, and the other named PBSRM has partial magnetic barriers of BSRM.

The configurations and common specifications of the two barrier-type SRM and the prototype are introduced at first. Then, the coupled field-circuit method, used for magnetic characteristic analysis of the three motors, is explained. After experimental results are presented to prove the accuracy of the method, the several analysis results of the three SRM are compared, and the effective magnetic barrier shape is presented.

II. SPECIFICATIONS AND CONFIGURATIONS

A prototype, which is made for study at Changwon National University in Korea, has been used as the basis for designing the barrier type motors used in this comparison. Table I shows the common specifications.

The two barrier-type SRMs are identical with the prototype except the existence of magnetic barrier in the rotor. The rotors of prototype and barrier-type SRM which have inserted magnetic flux barrier are shown in Fig. 1. The magnetic flux barrier is divided into two parts, pole barrier and link barrier. If the rotor has both pole barrier

and link barrier, the motor is called BSRM, and if it has only pole barrier, the motor is called PBSRM in this paper. For BSRM, the magnetic barriers have been optimized by response surface methodology to increase average torque and reduce torque ripple [1]. The PBSRM has partial magnetic barriers of BSRM. The barrier shape of PBSRM is designed by considering magnetic flux paths of general SRM so that main flux path directly crosses the rotor to each counter part pole when the switches are turned on and off by phases. The three models' wire-cut segments are shown in Fig. 2.

As a controller circuit, non-symmetric circuit as shown in Fig. 3 is used. Fig. 4 shows the switch on/off phase voltage and angle at the rated operating point. The base angle 0° is the position that stator and rotor poles are unaligned.

TABLE I COMMON SPECIFICATIONS

Parameter	Constraint
number of poles	stator : 8, rotor : 6
stator outer diameter	90.0 mm
rotor outer diameter	46.8 mm
rotor stack length	95.0 mm
air gap length	0.4 mm
stator pole arc	18.5°
rotor pole arc	19.0°
rated speed	1800 rpm
rated output power	260 W

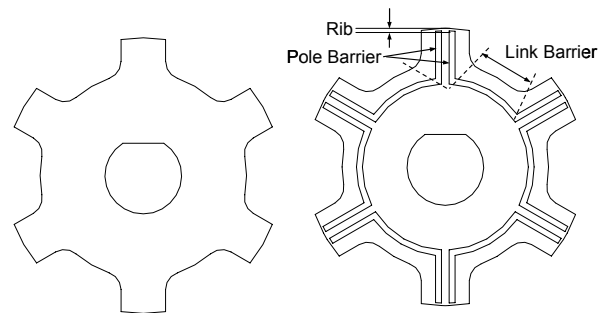


Figure 1. Configurations of prototype and barrier type rotors



(a) Prototype (b) BSRM (c) PBSRM

Figure 2. SRM configurations in comparison

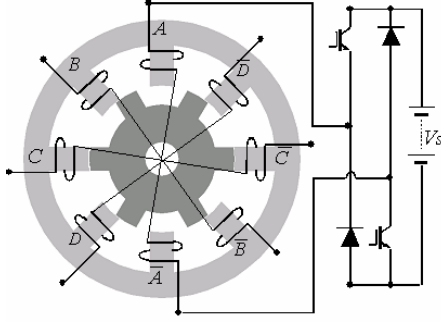


Figure 3. Controller circuit with 2 transistors per phase

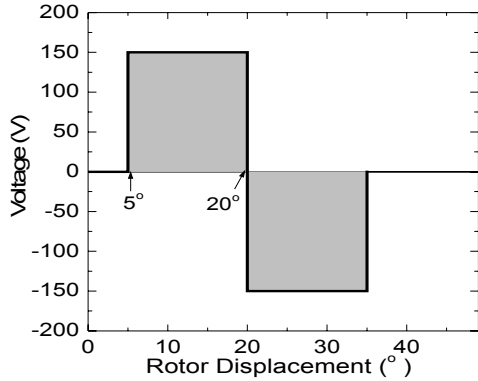


Figure 4. Input voltage (switch turn on/off angles: 5°, and 20°)

III. FIELD COMPUTATION METHOD

The electromagnetic characteristics of the SRM are computed by so-called coupled field-circuit method. For the coupled field-circuit method, 2D finite element method is used to model the nonlinear magnetic field of the SRM, and coupled to the power electronic circuit. For more accurate analysis, experimental equation is additionally used in order to consider the end-coil effect such as fringing effect.

A. Coupled Field Circuit Analysis

In order to reliably analyze the characteristics of the three models, not only complicated flux pattern of them, but also its terminal characteristics should be considered. To solve terminal equations and the flux equations at the same time, the coupled field circuit modeling method is effective [2].

The magnetic field of the SRM is governed by the 2D Poisson equation as following.

$$\frac{\partial}{\partial x} \left(v \frac{\partial A_z}{\partial x} \right) + \frac{\partial}{\partial y} \left(v \frac{\partial A_z}{\partial y} \right) = -J_0 \quad (1)$$

By solving this magnetostatic equation, the internal distribution of the magnetic field can be obtained. However, the winding currents which determine the current density, J_0 , must be known for solving the equations.

The terminal voltage equations of the SRM can be easily written according to the circuit configuration of the system. For four-phase stator windings, the voltage equation is as following.

$$v_{abcd} = r i_{abcd} + \frac{d\lambda_{abcd}}{dt} \quad (2)$$

where $v_{abcd} = (v_a, v_b, v_c, v_d)^T$ are the terminal voltages across the stator windings; $i_{abcd} = (i_a, i_b, i_c, i_d)^T$ are the phase currents of the stator windings; $\lambda_{abcd} = (\lambda_a, \lambda_b, \lambda_c, \lambda_d)^T$ are the flux linkages of the stator windings; and r is the winding resistance of the stator. ‘T’ indicates a transposed matrix. To find terminal current, the flux linkage variation as a function of time must be known.

Between (1) and (2), there are relations of variables. Current vector, i_{abcd} in (2) is related to the current density J_0 in (1), and flux linkage vector, λ_{abcd} , is related to the vector potential A_z . In the coupled modeling method, the (1) and (2) are to be solved simultaneously by numerical iterations. A matrix of equations contained in (1) is discretized into elemental form over the entire SRM cross-section as usual in finite element analysis for magnetostatic field analysis.

To discretize (2), one critical problem is to discretize the time derivatives, $d\lambda_{abcd}/dt$. The time derivative is replaced by the backward difference. That is as follows.

$$\begin{aligned} \frac{d\lambda_{abcd}}{dt} &= \frac{\Delta\theta}{\Delta t} \frac{d\lambda_{abcd}}{d\theta} \\ &= w_r \frac{\lambda_{abcd}(\theta, t_\theta) - \lambda_{abcd}(\theta - \Delta\theta, t_{\theta - \Delta\theta})}{\Delta\theta} \end{aligned} \quad (3)$$

where, $w_r = \Delta\theta/\Delta t$. As clearly indicated by (3), the time derivative terms are properly discretized. Then, the global equation set containing (1) and (3) can be obtained and solved simultaneously, provided that the terminal voltages V_{abcd} and detailed geometry of the SRM are given.

Fig. 5 shows the computation flow chart used for the coupled field circuit analysis modeling method of the SRM. Two major loops are designed in the algorithm, the inner current loop and the outer rotor position loop.

Note Δv , included in the inner current loop, is the difference between the actually applied voltage and the computed voltage from (2) for the current assumed. As soon as Δv falls within the predetermined error, the currents assumed converge to their true values which, in turn, determine the field vector potential of the SRM. If constant current is given to system, the current loop can be skipped except the step of field analysis by FEM in the flow chart.

B. End Winding Effect

By 2D FEM, the end winding effect can not be considered. In order to remedy this problem, some experimental equations can be used depending on the coil shapes [3],[4]. One example is the equation (4), which is used for calculation of end coil inductance per phase, L_{end} , in switched reluctance motors [4].

$$L_{end} = (N_p / P_{th}) \times \mu_0 a N_{ss}^2 \ln(8a / GMD - 2) \quad (H) \quad (4)$$

where N_p is number of turns per pole, P_{th} is number of parallel paths in the phase winding, a is coil radius, N_{ss} is number of pole-coils in series per phase, and GMD is geometric mean distance of coil side cross-section.

IV. EXPERIMENTAL TESTING VERIFICATION

2D FEM by a program named EMF, developed by ECAD Lab, is used in the computation procedures. Several analyses and experiments have been conducted on the three models. The basic specifications of the prototype are listed in Table I.

The 2D geometry of the SRM and the equipotential lines are shown in Fig. 6. As shown in these figures, the rotor poles of BSRM are more saturated than the others because of magnetic flux barriers. This saturation affects inductance profiles as shown in Fig. 7, in which the inductance profiles are changed according to current, rotor displacement, and barrier shape. The displacement represents the rotor position. 0° denotes the position where stator pole and rotor pole are unaligned and 30° denotes the position where the rotor pole is aligned to the current excited stator pole.

A. Experiment at Current Operation Mode

In Fig. 7, the analysis data is obtained by coupled field modeling method at constant current condition for which the current loop is skipped except the step of field analysis by FEM in the flow chart. It is seen that even at the same conditions of current and rotor displacement, the inductance profiles are distorted by magnetic flux barrier shape.

The experimental results are obtained from a measuring method of AC power at constant current. With AC power, the inductance was calculated by measured voltage, V_{rms} , current, I_{rms} , and phase angle, θ using Eq. (5).

$$R = \frac{V_{rms} \cos \theta}{I_{rms}}, L = \frac{V_{rms} \sin \theta}{\omega I_{rms}} = \frac{V_{rms} \sin \theta}{2\pi f I_{rms}} \quad (5)$$

where, the frequency, f , is 50Hz in the test.

The analytical and experimental inductances are in substantial agreement as shown in Fig. 7. The results give reliance on the input data, FEM as field analysis method, and consequently the rotor position loop in the flow chart, Fig. 3.

B. Experiment at Voltage Operation Mode

Fig. 8 shows the comparison of calculated and measured currents of prototype. The calculated result is obtained by coupled field modeling method at switch turn-on voltage 80V, turn-off voltage 150V, and speed 800 rpm. The measured current is obtained by computer controlled DSP driver under the same condition. By this comparison, it is noted that the simulation results has a good agreement with the experimental results. It is clear that the current waveform predicted by the coupled field circuit modeling method is in a very good agreement with that from the testing. Therefore, reliable assessment is possible by the comparison of the analysis results.

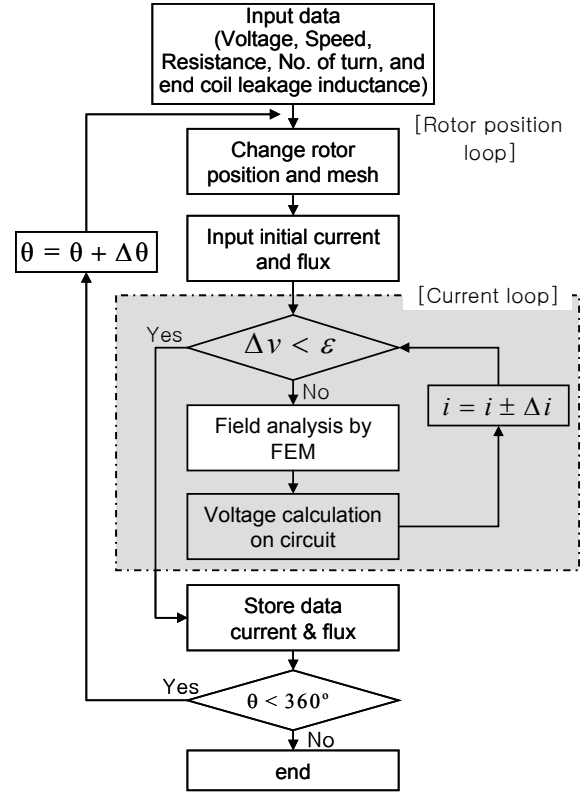
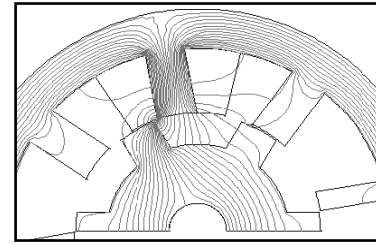
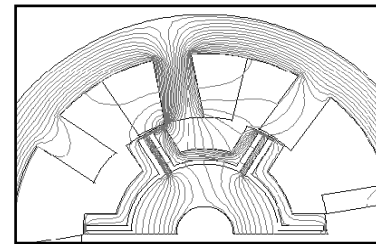


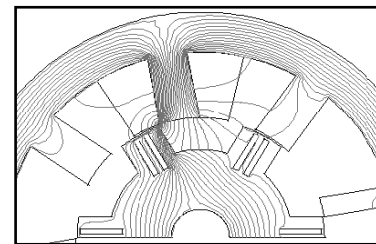
Figure 5. Flow chart of coupled field modeling method



(a) Prototype

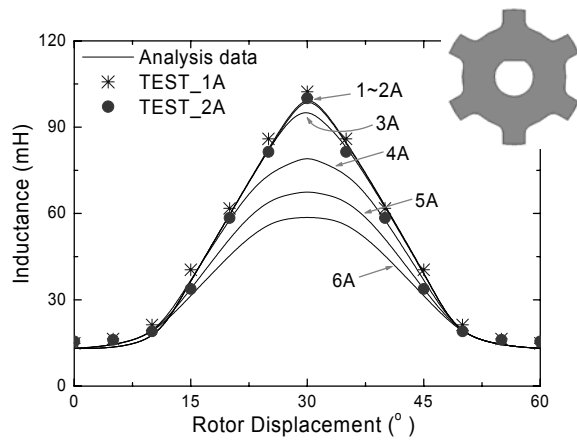


(b) BSRM

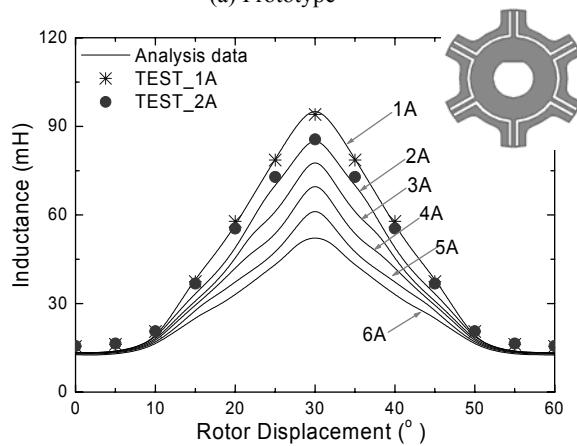


(c) PBSRM

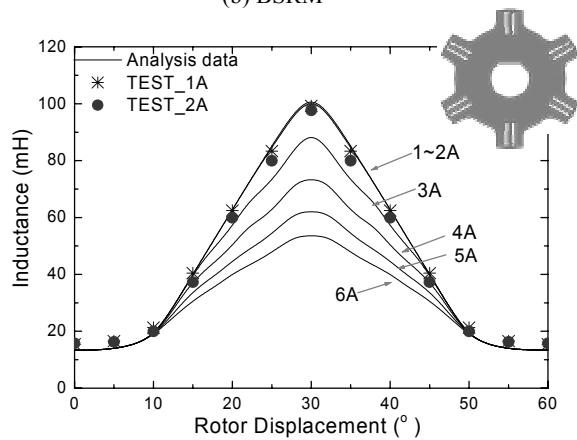
Figure 6. Equipotential line of three models



(a) Prototype



(b) BSRM



(c) PBSRM

Figure. 7 Comparison of inductances

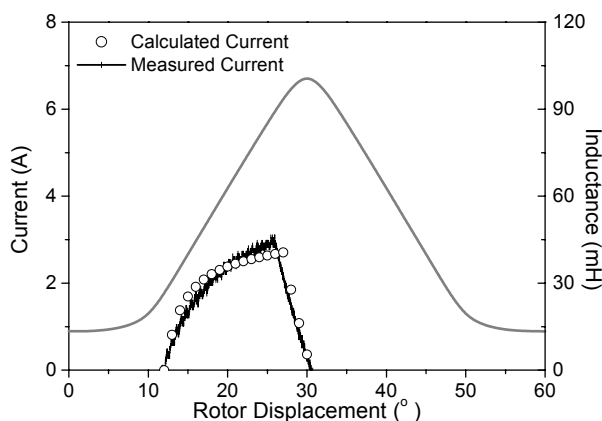


Figure 8. Comparison of Currents

V. COMPARISONS OF PERFORMANCES

From Fig. 9 to Fig. 11 show the comparison of analysis results for three models by the coupled field circuit modeling method. The analysis conditions at the speed of 1800rpm are the same as those of rated condition of prototype as mentioned in table I.

It is noted that although the input voltage maintained constant for 15° , rotor position, the phase current fluctuates over 1A after reaching its peak value at about 12° . Furthermore, the peak current does not correspond to the instant when the maximum flux linkage occurs. After the transistor is turned off, the phase current takes a sit of time to decay. Despite of the same operating condition, the current fluctuations are different because of distorted inductance due to the magnetic barriers. When the rotor moves towards the alignment with the stator, the rotor poles start to be saturated, and inductance profile of prototype become curved. However, the inductance profiles of BSRM become so straighter under saturation condition that the current can keep the plate top shape during switch turn-on period. For PBSRM, the inductance profile is also curved, but its direction is opposite to that of prototype. That causes different current fluctuating shape.

Consequently the torque characteristics are different from each other because the different current and inductance profiles. According to this comparison, BSRM has less torque ripple than prototype does at rated speed 1800 rpm

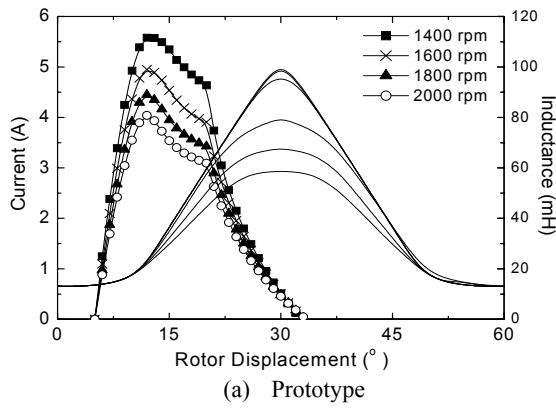
Fig. 12 and Fig. 13 show the torque characteristics of the three models according to speed variation 1000-2000 rpm. The input conditions such as input voltage and switch turn-on and off angle are the same as in Table I. It is noticeable that even though the output power is identical with each other at high speed, the torque ripples are quite different. The difference of torque ripple between prototype and barrier type SRM, PBSRM and BSRM, is increased as speed increases. Therefore, the BSRM can be a good model to reduce torque ripple of SRM at high speed.

VI. CONCLUSIONS

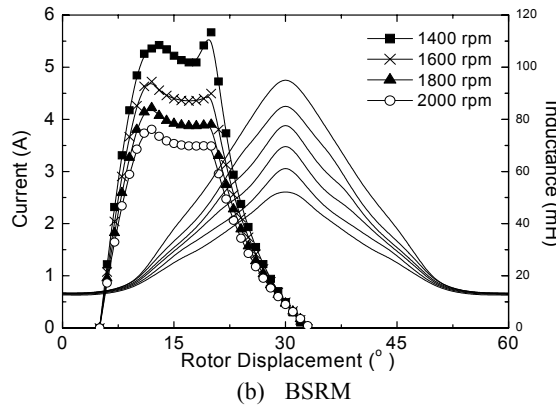
This paper dealt with two kinds of SRM with inserted magnetic flux barriers in order to improve operating performances of prototype, and the coupled field circuit modeling method was used to reliably evaluate the characteristics of the motors.

By experimental results, it is evaluated not only validation of the FEM and the coupled field circuit analysis method, but also effect of magnetic flux barrier due to changed inductance profiles. And the results obtained by the coupled field circuit analysis method show that the SRM with magnetic flux barriers can reduce torque ripple.

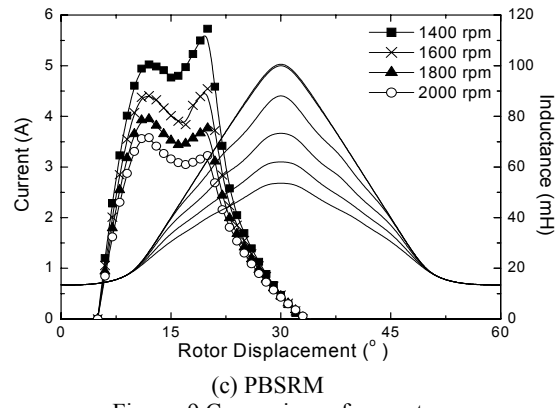
In design of SRM considering control, the magnetic flux barrier can be the important element, and these results can be used useful references.



(a) Prototype

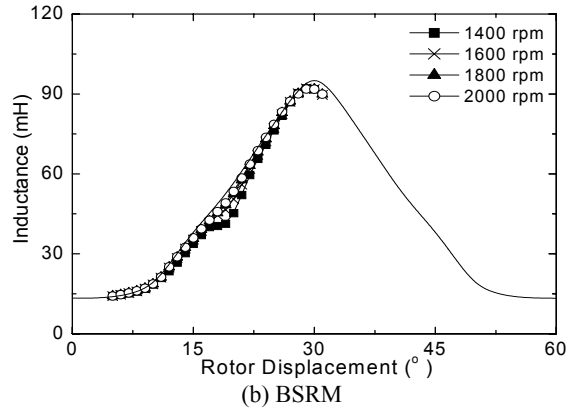


(b) BSRM

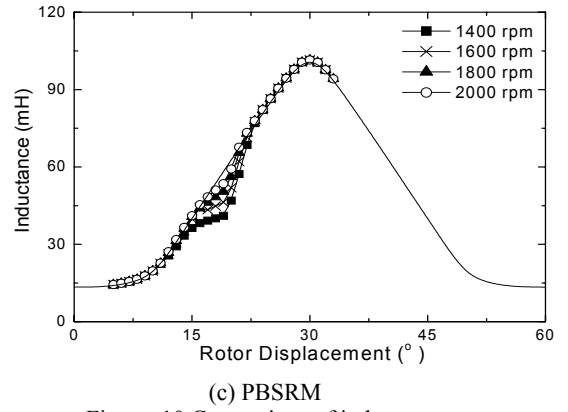


(c) PBSRM

Figure. 9 Comparison of current

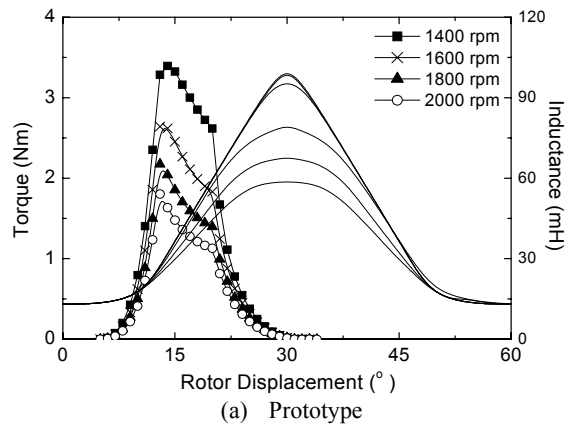


(b) BSRM

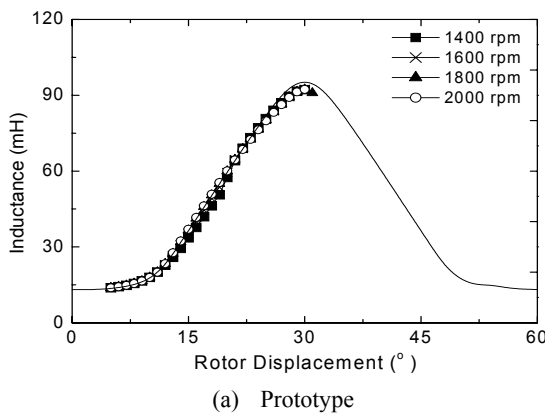


(c) PBSRM

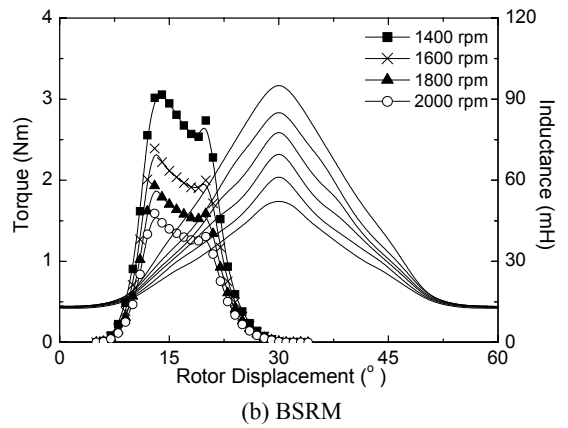
Figure. 10 Comparison of inductance



(a) Prototype



(a) Prototype



(b) BSRM

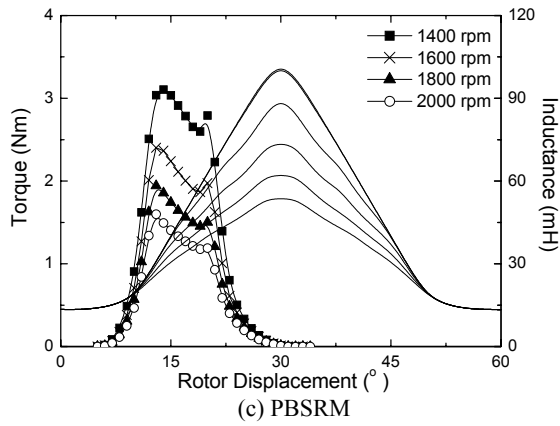


Figure 11 Comparison of one phase torque

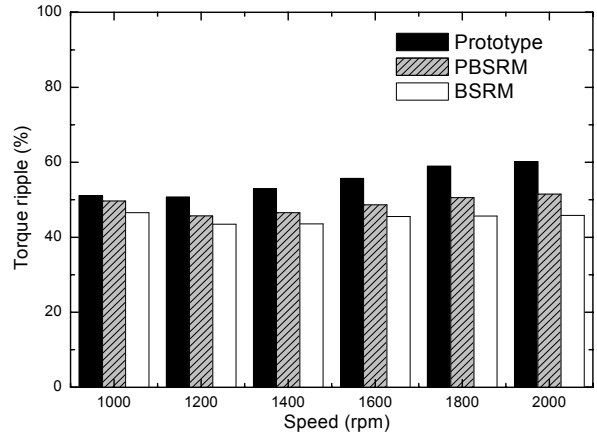


Figure 13. Torque ripple according to speed variation

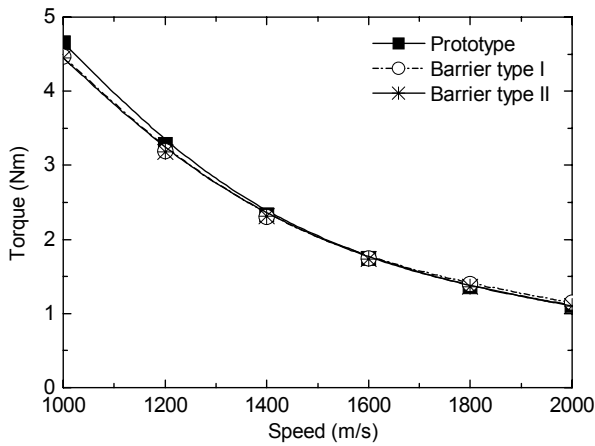
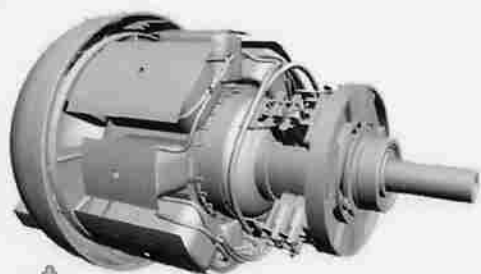


Figure 12. Average torque according to speed variation

VII. REFERENCES

- [1] Young-Kyoun Kim, Ji-young Lee, Jung-Pyo Hong, and Jin Hur, "Optimization of Barrier type SRMs with Response Surface Methodology Combined with Moving Least Square Method," *International Symposium on Electromagnetic Fields in Electrical Engineering (ISEF2003)*, vol.2/2, pp659-664, September 18-20, 2003, Maribor, Slovenia.
- [2] Longya Xu and Eric Ruckstadter, "Direct Modeling of Switched Reluctance Machine by Coupled Field-Circuit Method," *IEEE Trans. on Energy Conversion*, vol. 10, No. 3, pp446-454, September, 1995
- [3] TJE Miller, *SPEED Consortium PC-SRD version 7.0 Uwer's Manual*, University of Glasgow, June 1999
- [4] Frederick W. Grover, *Inductance Calculations*, D. Van Nostrand Company, Inc.

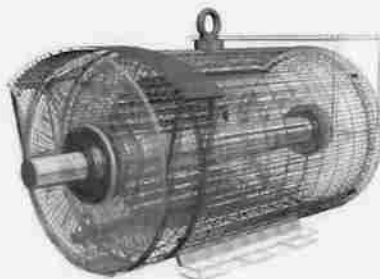
16th International Conference on Electrical Machines



ICEM 2004



5-8 SEPTEMBER 2004, CRACOW - POLAND



BOOK OF DIGESTS

vol 1

Editors: S. Wiak, M. Dems, K. Komeza

iMSI

**Institute of Mechatronics and Information Systems
Technical University of Lodz, Poland**

PS2-21	Fractional-Slot IPM Servomotors: Analysis and Performance Comparisons.....	173
	<i>N. Bianchi, S. Bolognani, G. Grezzani</i>	
PS2-22	Electric Motors Featuring Multiple Degrees-of-Freedom	175
	<i>P. Bolognesi, O. Bruno, A. Landi, L. Sani, L. Taponecco</i>	
PS2-23	Performance Analysis of a Solid Rotor Disk Induction Motor	177
	<i>S.E. Abdollahi, M. Mirsalim, M. Mirzayee</i>	
PS2-24	Increase Armature Voltage for the Superconducting DC Motor.....	179
	<i>D. Wu, J. Chen</i>	
PS2-25	Low-Stiffness Motor: Review of Different Ironless Motors Topologies for Use in Precision Engineering Applications.....	181
	<i>M.H. El-Husseini, J.W. Spronck, H. Polinder, H.H. Langen, J. van Eijk</i>	
PS2-26	Design to Improve Starting Capability of Single-Phase Line-Start Synchronous Reluctance Motor ...	183
	<i>Hyuk Nam, Su-Beom Park, Jung-Pyo Hong, Tae-Uk Jung, Jae-Boo Eom</i>	
PS2-27	Optimal Design for Volume Reduction of Nd-Fe-B Magnet in BLDC Motor	185
	<i>Sang-Joon Han, Hong-Soon Choi, Il-Han Park</i>	
PS2-28	New Development of Multifunction Device for 4 Different Functions in Mobile Phones	187
	<i>Sang-Moon Hwang, Hong-Joo Lee, Keum-Shik Hong, Beom-Soo Kang, Gun-Yong Hwang</i>	
PS2-29	Magnetic Barrier Effect on Operating Performances of Switched Reluctance Motor	189
	<i>J.Y. Lee, K.Y. Nam, Jung-Pyo Hong, J. Hur</i>	
PS2-30	Steady State Model of the Single-Phase Capacitor-Run Hybrid Induction Motor	191
	<i>Sun-Ki Hong</i>	
PS2-31	Simulation and Experimentation of a Two-Phase Claw-Pole Motor	193
	<i>A. Reinap, M. Alaküla</i>	
PS2-32	New Design of Switched Reluctance Motor to Improve ITS Efficiency	195
	<i>P. Rafajdus, V. Hrabovcová, M. Lipták, I. Zrak</i>	
PS2-33	Induction Motors with Spherical Rotor	197
	<i>G. Kamiński, A. Smak</i>	
PS2-34	Design and Optimisation of Brushless Integrated Starter-Generator	199
	<i>L. Gašparin, R. Fišer</i>	
PS2-35	Simulation and Experimentation of a Single-Phase Claw-Pole Motor	201
	<i>A. Reinap, M. Alaküla, G. Nord, L.O. Hultman</i>	
PS2-36	Optimal Excitation Parameters of a Single-Phase SR Generator.....	203
	<i>M. Lipták, P. Rafajdus, V. Hrabovcová, I. Zrak</i>	
PS2-37	Comparison of Brushless DC Motors with Concentrated Winding and Segmented Stator.....	205
	<i>J. Cros, P. Viarouge, R. Carlson, L.V. Dokonal</i>	

vol 2

Special Machines

OS4		
OS4-1	Design of a High Speed Permanent Magnet Brushless Generator for Microturbines	209
	<i>J.F. Gieras</i>	
OS4-2	Variable Pole, Variable Phase Machines	211
	<i>M. McCulloch</i>	
OS4-3	Asynchronous Wheel Hub Motor with Massive Rotor Iron and Open Rotor Slots for Wheel Hub Drives in Street Cars	213
	<i>W. Hackmann, A. Binder</i>	
OS4-4	Control of Switched Reluctance Machines for Flywheel Energy Storage Applications	215
	<i>M. Holub, R. Palka, W.R. Canders</i>	
OS4-5	Study on Magnetic Field and Output Voltage of Axial Type Generator for Wind Power Generation ...	217
	<i>E. Mukai, S. Washimiya</i>	
OS4-6	Electrostatic Synchronous Motors	219
	<i>M. Crivii, M. Jufer</i>	